Effect of stratification on the turbulent wake behind a sphere at Re = 10,000

Karu Chongsiripinyo

Department of Mechanical
and Aerospace Engineering
University of California, San Diego
9500 Gilman Dr, La Jolla, CA 92093
kchongsi@eng.ucsd.edu

Sutanu Sarkar

Department of Mechanical
and Aerospace Engineering
University of California, San Diego
9500 Gilman Dr, La Jolla, CA 92093
sarkar@ucsd.edu

ABSTRACT

Large eddy simulation of flow past a sphere in a density-stratified fluid is performed at a Reynolds number of $Re = U_\infty D/\nu = 10{,}000$ and $Fr = U_\infty/ND = \infty$, 3, and 1 where $Fr = \infty$ refers to the unstratified case. Here, U_∞, D, and N are the free-stream velocity, sphere diameter, and constant background buoyancy frequency, respectively. The choice of $Fr = O(1)$ allows investigation of the turbulent wake under conditions where the buoyancy time scale, $1/N$, is comparable to the mean flow time scale, D/U_∞. Visualizations in the form of Q-criterion and azimuthal vorticity show that stratification introduces qualitative changes in the near wake structure as well as the helical mode instability. The centerline defect velocity, U_0, in the unstratified wake decays according to the power law, $U_0 \propto x^{-m}$, with $m = 1$ instead of the classical value of $m = 2/3$. In the stratified wakes, U_0 exhibits an "oscillatory modulation" owing to the lee-wave pattern created by the sphere. As a result, U_0 increases in the region $\pi Fr \leqslant x/D \leqslant 2\pi Fr$ instead of the usual decrease. Further downstream, there is an overall decrease of U_0 but the exponent m in the power law, $U_0 \propto x^{-m}$, is reduced to $m = 0.4$. The turbulent kinetic energy ($t.k.e.$) budget is quantified to assess the influence of stratification. The relative roles of advection, production, dissipation, transport and buoyancy flux are found to be altered over the entire wake at $Fr = 1$ and in the intermediate and far wake at $Fr = 3$.

INTRODUCTION

Turbulent wakes under stratification are ubiquitous, e.g. in flows past marine swimmers, underwater submersibles, underwater topography, islands and mountains. In the early years, stratified wakes were studied primarily using experimental methods. Early experiments, as reviewed in Lin & Pao (1979), showed that stratification suppresses vertical motion, promotes downstream horizontal coherent eddies, and enables propagation of internal gravity waves into the far field. With better experimental instruments and advances in numerical simulation, more accurate qualitative and quantitative results have been obtained. Chomaz *et al.* (1993) experimentally showed that stratified wakes can be divided into four different regimes based on $Fr = U/ND$. For $Fr < 0.4$, the wake corresponds to triple-layer flow with two lee waves surrounding a layer of two-dimensional motion. For Fr between 0.4 and 0.75, the saturated lee wave suppresses the separation region or splits it into two. When Fr is between 0.75 and 2, the buoyancy effect on the near wake progressively decreases in importance and, by $Fr > 2.25$, the near wake is similar to the homogeneous case. A stratified wake at high Fr ($Fr > O(1)$) exhibits three distinct regions. The first region is the near wake (NW) where the wake spreads uniformly in all directions and turbulence behaves as it does in a homogeneous fluid. It is followed by a second non-equilibrium (NEQ) regime identified by Spedding (1997) where there is an onset of buoyancy effects including conversion of stored potential energy to kinetic energy and anisotropy between horizontal and vertical motions. The third region (Q2D) is characterized by the existence of vertically suppressed two-dimensional eddies, so called "pancake vortices".

Recently Pal *et al.* (2016) and Pal *et al.* (2017) performed DNS of stratified flow past a sphere at $Re = 3700$ over a wide range of stratifications that encompass the $Fr < O(1)$ regime, the $Fr = O(1)$ regime and the lower boundary of the $Fr > O(1)$ regime. Unlike previous DNS/LES of stratified wakes that used a temporal flow model (Brucker & Sarkar (2010); Diamessis *et al.* (2011)), the body was included in these simulations. Though computationally expensive owing to resolution of the boundary layer, the simulation led to new results regarding the near and intermediate wake. It was found that the body-generated lee waves cause oscillatory modulation of the mean defect velocity. Also, the flow enters a new regime of horizontal vortex shedding and turbulence when Fr smaller than about 0.25.

The objective of the present paper is to examine stratified and unstratified flow past a sphere at a higher $Re = 10^4$ and contrast the results with our knowledge of the $Re = 3700$ wake. We address the following questions. Do decay rates of centerline defect velocity change at higher Re? Do oscillatory modulations persist at the higher Re? What qualitative and quantitative changes occur in the turbulent kinetic energy budget?

EQUATIONS

A sphere of diameter D is immersed in a stream with velocity U. The background is density-stratified with a constant vertical density gradient, $d\rho_b/dx_3$, and buoyancy frequency N that is defined by $N^2 = -(g/\rho_o)d\rho_b/dx_3$ with ρ_0 a reference density that is representative of the background. The filtered Navier-Stokes equations under the Boussinesq approximation for density effects are solved along with an advection-diffusion equation for the filtered density. A dynamic eddy viscosity model is utilized. The following system of non-dimensional governing equations is numerically solved.

Continuity:

$$\frac{\partial u_i}{\partial x_i} = 0, \tag{1}$$

Momentum:

$$\frac{\partial u_i}{\partial t} + u_j \frac{\partial u_i}{\partial x_j} = -\frac{\partial p}{\partial x_i} + \frac{1}{Re}\frac{\partial}{\partial x_j}\left[\left(1 + \frac{\nu_{sgs}}{\nu}\right)\frac{\partial u_i}{\partial x_j}\right] - \frac{1}{Fr^2}\rho_d \delta_{i3}, \tag{2}$$

Density:

$$\frac{\partial \rho}{\partial t} + u_j \frac{\partial \rho}{\partial x_j} = \frac{1}{Re}\frac{\partial}{\partial x_j}\left[\left(1 + \frac{\nu_{sgs}}{\nu}\right)\frac{\partial \rho}{\partial x_j}\right]. \tag{3}$$

In Eq. (2), ρ_d is the deviation of the density from the background density, $\rho_b(x_3)$. Here, ν is the constant kinematic viscosity and κ is the constant diffusivity of density while ν_{sgs} and κ_{sgs} are the subgrid transport coefficients introduced by the LES model. The fluid has molecular Prandtl number, $Pr = \nu/\kappa = 1$, and the subgrid $Pr_{sgs} = \nu_{sgs}/\kappa_{sgs}$ is assumed to be unity leading to the simplified form of the RHS of Eq. (3). The Froude number, $Fr = U/ND$, and the Reynolds number, $Re = UD/\nu$, are the primary non-dimensional parameters. In the following discussion, all variables discussed are non-dimensional unless otherwise noted. Subgrid viscosity, ν_{sgs}, is obtained using the dynamic eddy viscosity model of Germano *et al.* (1991). The coefficient C, as in $\nu_{sgs} = C\overline{\Delta}^2|\overline{S}|$, is dynamically computed using a method of Lilly (1992). C is dynamically averaged along flow trajectories with an exponential weighting function chosen to give more weight to recent times in flow history.

NUMERICAL METHOD

Governing equations (1)–(3) are solved numerically in a cylindrical coordinate system on a staggered grid. The sphere is represented by the immersed boundary method of Balaras (2004); Yang & Balaras (2006). The equations are marched using a combination of explicit and implicit schemes. Implicit marching by the second order Crank-Nicolson (CN) scheme is performed for the terms in the azimuthal direction to alleviate stiffness of the discretized system. The remaining terms are marched explicitly using a third-order Runge-Kutta (RK3) scheme. A periodic boundary condition in the azimuthal direction transforms the discretized Poisson equation into inversion of a pentadiagonal matrix. The pentadiagonal matrix system is solved using a direct solver, Rossi & Toivanen (1999). Inflow and convective outflow boundary conditions are applied at the inlet and outlet of the domain. In order to control spurious reflections from internal waves and other disturbances propagating out of the domain, sponge regions are employed near the free stream and inlet boundaries where the following relaxation terms are added to the governing equations:

$$-\phi(x_i)[u_i(x_i,t) - U_i], \qquad -\phi(x_i)[\rho(x_i,t) - \rho_\infty(x_3)]. \quad (4)$$

The sponge layer takes the form of a Rayleigh damping function which is designed in such a way so as to gradually relax the velocities and density to their respective values at the boundaries. Here U_i is the freestream velocity and $\rho_\infty(x_3)$ is the density of the stratified background. This is accomplished by adding the explicit damping terms of equation (4) to the right hand side of equation (2) and (3). The variable $\phi(x_i)$ is constructed such that it increases quadratically from $\phi = 0$ to $\phi = 1$ over a sponge region of thickness 10 grid points at the inflow and at the freestream boundaries.

PARAMETERS

All simulations are performed with $Re = UD/\nu = 10^4$. Three cases are investigated with $Fr = \infty$ (unstratified), $Fr = 3$, and $Fr = 1$. The choice of $Re = 10^4$ allows for validation against the LES of Rodríguez *et al.* (2013), Yun *et al.* (2006), and Constantinescu & Squires (2004). Domain sizes in the upstream, downstream, and radial directions are $L_x^-/D = 40.16$, $L_x^+/D = 80.62$, and $L_r/D = 59.84$, respectively. The sphere center is at $(x/D, r/D) = (0,0)$. In comparison to the unstratified flow past a sphere of Rodríguez *et al.* (2013), the domain sizes in the radial and upstream directions are enlarged to allow free propagation of internal gravity waves induced by stratification. While this is not necessary for the unstratified case, the same domain size is kept for consistency. The number of grid points in the streamwise, radial, and azimuthal directions are $N_x = 6144$, $N_r = 918$, and $N_\theta = 128$ giving a total number of
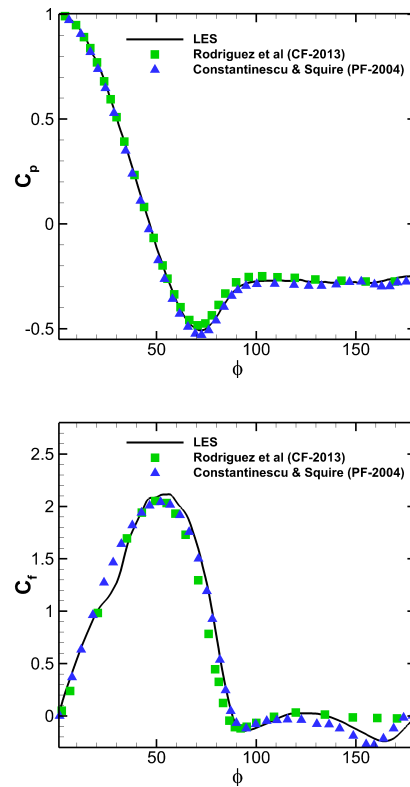
Figure 1. Temporal-azimuthal average of pressure coefficient and shear stress on the sphere.

grid points of approximately 720 million. Grid stretching is used in the radial and streamwise directions to concentrate points near the sphere surface in order to resolve the laminar boundary layer. To compute statistics, temporal averaging of data is performed over 100 non-dimensionalized time units or approximately one flow-through time unit after statistical steady-state. Each simulation uses 512 processors with approximately 1700 hours of wall clock time. The computations utilize a Cray XC40 system with Intel Xeon E5-2698v3 (Haswell-EP) processors clocked at 2.3 GHz.

VALIDATIONS

Validation of the unstratified case is performed by examination of the distributions of mean pressure coefficient and mean skin friction coefficient on the body, mean separation angle, drag coefficient and shedding frequency. Computation of the mean is done by averaging both in time and in the azimuthal direction. These results are compared with previous results (Rodríguez *et al.* (2013) and Constantinescu & Squires (2004)). Figure 1 shows that pressure and skin friction coefficients are well captured in our simulation. The variable ϕ in the figure denotes the angle from the forward stagnation point of the sphere, $\phi = 0$. Mean separation angle, ϕ_s, is determined by the position, ϕ, where mean $C_f = 0$. The minimum value of C_p, located at $\phi = 72^o$, marks the onset of an adverse pressure gradient. The rise in C_p beyond $\phi = 72^o$ indicative of this adverse gradient contributes to a continuous decrease in C_f until the flow detaches from the surface at separation angle of $\phi_s = 88.1^o$.

VISUALIZATIONS

Three-dimensional visualization of instantaneous vortical structures in the wake is done using the Q-criterion of Hunt *et al.* (1988), $Q = 0.5(|\mathbf{\Omega}|^2 - |\mathbf{S}|^2)$ where $\Omega_{ij} = 0.5\left(\partial u_i/\partial x_j - \partial u_j/\partial x_i\right)$ and $S_{ij} = 0.5\left(\partial u_i/\partial x_j + \partial u_j/\partial x_i\right)$. Figure 2 shows isosurface of

Studies	St	ϕ_s	C_d	C_{pb}
Present LES	0.199	88.1	0.407	-0.251
Rodríguez et al. (2013)	0.195	84.7	0.402	-0.272
Yun et al. (2006)	0.17	90	0.393	-0.274
Constantinescu & Squires (2004)	0.195	84	0.393	

Table 1. Comparision of near field statistics.

$Q = 2$, 1, and 0.5 for $Fr = \infty$, 3, and 1, respectively. The reduction of isosurface Q-level with increasing Fr is required to enable sufficient downstream extent of the wake-structure visualization. Regions with intensified fluid element rotation are signified by a large positive value of Q where the rate of rotation tensor, Ω_{ij}, exceeds the rate of strain tensor, S_{ij}. For the unstratified case in the range, $0.5 \leqslant x/D \leqslant 1$, axisymmetric vortex rings are shed from the sphere. Helical orientation of the unstratified wake previously observed by Yun et al. (2006) is apparent in Figure 2 (top). Visualization of the isosurfaces at different times confirms that helical structures do not rotate around the streamwise axis as they travel downstream but rather simply translate downstream as stated in Yun et al. (2006). At $Fr = 3$ and especially $Fr = 1$, the vortex rings are distorted into ellipsoids with the major axis in the spanwise, y, direction. The suppression of vertical motion is, thus, immediate for $Fr = O(1)$ wakes and influences how the incoming freestream travels around the sphere. In their results for stratified flow past a sphere at $(Re, Fr) = (3700, 0.5)$, Chongsiripinyo et al. (2017) visualized blocking in front of a sphere, i.e there is insufficient kinetic energy to vertically displace incoming fluid over the poles of the sphere. The incoming fluid is, thus, forced to travel horizontally around the sphere when $Fr < O(1)$.

Besides the helical orientation in the unstratified case, a wavy orientation is present at $Fr = 3$ but only in the horizontal plane while this feature disappears for $Fr = 1$. The number density of vortical structures in all cases decrease downstream. Chongsiripinyo et al. (2017) investigated dynamics of vortical structures by means of the enstrophy budget. Their results show that stretching/tilting of vorticity fluctuation by fluctuating strain, $\overline{\omega_i' \omega_j' s_{ij}'}$, is primarily responsible for the high density of vortical structures in a small region behind the sphere $1.5 < x/D < 5$.

Figure 3 and 4 show contours of instantaneous spanwise vorticity in the vertical center plane ($y = 0$) for $-1 < x/D < 10$ and $10 < x/D < 40$. For the unstratified case, given that the present $Re = 10^4$ is much smaller than the critical Reynolds number, $Re \sim 3 \times 10^5$, the entire boundary layer remains laminar from the forward stagnation point until separation. The separated shear layer breaks down into small scale motions via Kelvin-Helmholtz (KH) instabilities at the separated shear layer for both $Fr = \infty$ and 3. At $Fr = 1$, the separated shear layers initially conform with lee waves that have higher amplitude than those at $Fr = 3$; consequently, the shear layers bend toward the centerline. The location where the shear layers plunge at the centerline is also where production of $t.k.e$ achieves its maximum. The $t.k.e.$ budget is explained in a subsequent section. Figure 4 shows not only the apparent vertical suppression but also the gradual disappearance of small-scale eddies as stratification increases. Internal gravity waves emitted from the wakes are also detected in both stratified cases.

DEFECT VELOCITY

Figure 5 shows the temporal mean streamwise defect velocity at the centerline. There is an initial rise of defect velocity for all cases close to the sphere in the recirculation zone. For the unstratified case, after the peak, the defect velocity monotonically decreases and approaches an approximate constant decay
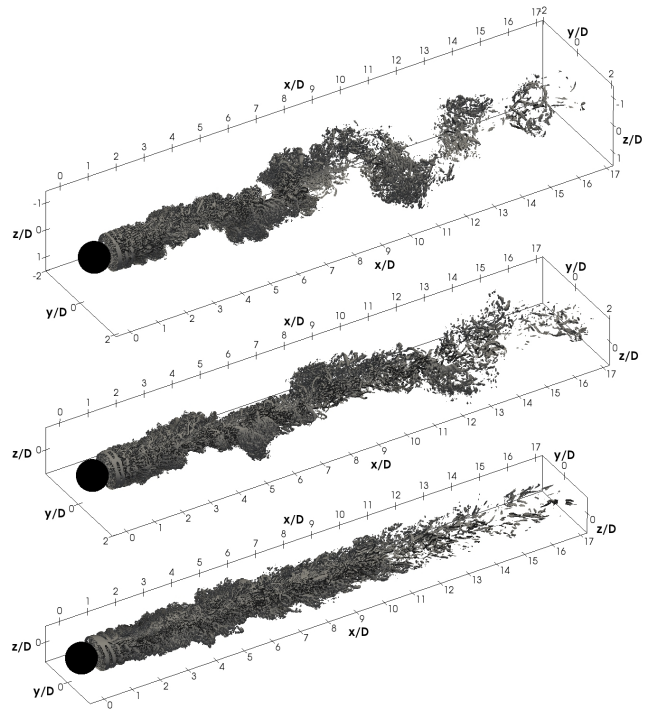
Figure 2. Isosurface of Q for $Fr = \infty$ (top, Q=2), $Fr = 3$ (middle, Q=1), and $Fr = 1$ (bottom, Q=0.5).
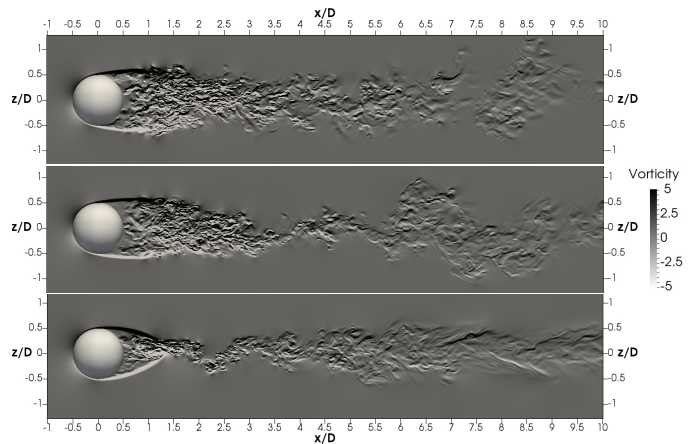
Figure 3. Spanwise vorticity contour in the near wake ($-1 < x/D < 10$) on a vertical plane for $Fr = \infty$ (top), $Fr = 3$ (middle), and $Fr = 1$ (bottom).

rate of $(x/D)^{-1}$. This $(x/D)^{-1}$ power law is also observed in an unstratified flow past a sphere at lower $Re = 3700$ in Pal et al. (2017). The equilibrium similarity analysis of axisymmetric wakes from George (1989) has shown that the $(x/D)^{-1}$ decay rate of defect velocity can be derived from the low Re dissipation scaling, $D_0 \sim \nu u_0^2/\delta^2$, where u_0 and δ are the characteristic velocity and length scale, respectively. However, this dissipation scaling is not valid in high-Re flow with fully developed turbulence. Recently, Nedić et al. (2013) introduced a modified dissipation scaling, $D_0 \sim (U_\infty l/\nu)^m (u_0 \delta/\nu)^{-n} u_0^3/\delta$ where l is the size of the wake generator. By setting $m = n = 1$, they obtain $U_0 \sim (x/D)^{-1}$ which, in contrast to George (1989), is independent of global Reynolds number $Re_G = U_\infty l/\nu$.

Centerline defect velocities in stratified cases behave differ-
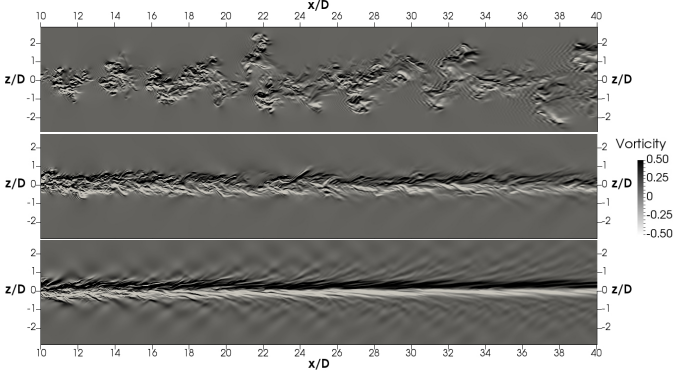
Figure 4. Spanwise vorticity contour in the intermediate ($10 < x/D < 40$) for $Fr = \infty$ (top), $Fr = 3$ (middle), and $Fr = 1$ (bottom).
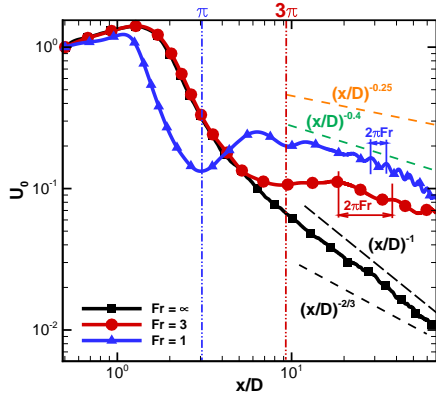
Figure 5. Centerline mean streamwise defect velocity.

ently from their unstratified counterpart. Distributions of the defect velocities over the streamwise centerline for both stratified cases contain information imposed by the body and the buoyancy frequency. Both velocities reach their first minimum at half of their buoyancy period, $x/D = \pi Fr$, away from the sphere center. Downstream of the first minimum, the defect velocity, U_0, increases and reaches a peak at one full buoyancy period, $x/D = 2\pi Fr$. Bonnier & Eiff (2002) used hot-film measurement and identified a region known as "accelerated collapse" which is characterized by an increase in defect velocity until achieving a so-called transition region where the defect velocity starts to decrease again. The "accelerated collapse" is better termed "oscillatory modulation" and the initial increase of U_0 occurs in the region $\pi Fr \leqslant x/D \leqslant 2\pi Fr$. In fact, the defect velocities in both stratified cases continue to alternately increase and decrease further downstream in response to the steady lee-wave pattern created by the sphere. These oscillatory modulations especially those downstream are also visible for lower $Re = 3700$ as in Pal et al. (2017). Beyond $x/D = 2\pi Fr$, the defect velocities decay with an overall trend $U_0 \propto x^{-m}$ where $m \simeq 0.4$. Bonnier & Eiff (2002) report $m = 0.38$ in their stratified flow past a sphere experiments with $(Fr = U/ND, Re) = (1.5, 3400); (3, 6900); (5, 11500)$. The fact that the decay rate of defect velocity in the stratified wakes is smaller than that of the unstratified wake implies that stratified wakes live longer in the mean.

TURBULENT KINETIC ENERGY

The evolution of turbulent kinetic energy is given below. This $t.k.e.$ budget details the energy dynamics from the fluctuating flow components. It is used to quantify and analyze the relative roles of advection, production, dissipation, transport, and buoyancy flux. The $t.k.e. = \langle u_i' u_i' \rangle / 2$ is denoted as K from here on.

$$\frac{\partial K}{\partial t} = A + P + \varepsilon + T + B \tag{5}$$

A and P are advection and production terms defined as,

$$A = -\langle u_j \rangle \frac{\partial K}{\partial x_j}, \qquad P = -\langle u_i' u_j' \rangle \frac{\partial \langle u_i \rangle}{\partial x_j} \tag{6}$$

ε, the turbulent dissipation rate and B, the buoyancy flux, are defined as follows.

$$\varepsilon = -\frac{1}{Re} \left\langle \left(1 + \frac{v_{sgs}}{v}\right) \frac{\partial u_i'}{\partial x_j} \frac{\partial u_i'}{\partial x_j} \right\rangle, \qquad B = -\frac{1}{Fr^2} \langle \rho_d' u_z' \rangle \tag{7}$$

T is the transport of K defined as,

$$T = -\frac{1}{2} \frac{\partial}{\partial x_i} \langle u_i' u_j' u_j' \rangle - \frac{\partial \langle p' u_i' \rangle}{\partial x_i}$$
$$+ \frac{1}{2Re} \left\langle \frac{\partial}{\partial x_j} \left(\left(1 + \frac{v_{sgs}}{v}\right) \frac{\partial (u_i' u_i')}{\partial x_j} \right) \right\rangle$$
$$+ \frac{1}{Re} \left\langle u_i' \frac{\partial u_j'}{\partial x_i} \frac{\partial (v_{sgs}/v)}{\partial x_j} \right\rangle \tag{8}$$

The cross-sectional area integrated terms in the turbulent kinetic energy budget are shown in Figure 7. For simplification, we divide the streamwise domain into 3 regions, $0.7 < x/D \leqslant 10$, $10 < x/D \leqslant 40$, and $40 < x/D \leqslant 70$ referred to as near, intermediate, and far wake, respectively. Note that this nomenclature is consistent with unstratified-wake literature and does not correspond to regimes based on buoyancy frequency.

The near-wake evolution of $t.k.e.$ (left column of Figure 7) reveals that the generation, destruction, and transport of $t.k.e.$ are relatively large close to the sphere, $0.7 \leqslant x/D \leqslant 5$. Both production and dissipation reach their peaks at approximately the same location of $x/D \simeq 1.5$. Integrated advection is initially negative in the vicinity of the recirculation region and, further downstream, is positive acting as a local source. The transport term, unlike in simulations of stratified flow past a sphere at lower $Re = 3700$ by Pal et al. (2017), is no longer negligible for the entire downstream domain regardless of Fr. Chomaz et al. (1993) points out that for $Fr > 2.25$, the near-wake is similar to the homogeneous case. Consistent with Chomaz et al. (1993), quantitative changes relative to the unstratified counterpart are largely insignificant in the $Fr = 3$ near-wake budget.

The near-wake balance of $t.k.e.$ is significantly altered at $Fr = 1$. The peak production is approximately 50% larger but large P spans a shorter streamwise distance so that the $t.k.e.$ shown in Figure 6 is smaller than in the unstratified case. The dissipation is significantly reduced so that at the point of maximum production, $P/\varepsilon \simeq 6$ compared to the unstratified-wake value of 2. There is a significant increase in advection. The maxima of production and advection occur at approximately the same location where the upper and lower separated shear layers plunge toward the centerline as observed in Figure 3. While the buoyancy term is negligible in the near wake of the $Fr = 3$ case, it is significant in the $Fr = 1$ case. B has an oscillatory signature that persists for the entire downstream domain. Note that since lee waves are introduced by a wake generator,
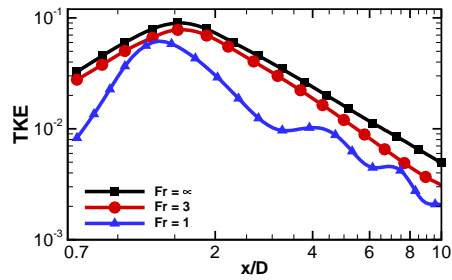
Figure 6. Area integrated turbulent kinetic energy.

a simulation using a temporal flow model, as in Brucker & Sarkar (2010), is unable to capture these oscillatory modulations in U_0, P and B. Buoyancy flux, B, as well as turbulent production, P, cross zero at $x/D = \pi$, the same location where the mean streamwise centerline defect velocity reaches its first local minimum. Thereafter, over the entire downstream region, both B and P show oscillations with wavelength of $2\pi Fr$. At $Fr = 3$, B and P also cross zero but in the intermediate wake and also exhibit oscillatory behavior. It appears that, in $Fr = O(1)$ wakes, the turbulent production crosses zero at $x/D \approx \pi Fr$ and, thereafter, both P and B exhibit an oscillatory modulation with spatial period of $2\pi Fr$.

The middle column of Figure 7 depicts the intermediate-wake region. In the unstratified case, production becomes small relative to the other terms and the flow evolves as freely decaying turbulence. Although shear production is also small in the stratified wakes, there are clear differences in the behavior of the different terms in the $t.k.e.$ balance. At $Fr = 3$, advection decreases by an approximate factor of two while the transport term becomes smaller by an even larger proportion. In addition, oscillatory modulations of buoyancy and production are visible. Dissipation is the only term which does not show the oscillatory signature but monotonically decays. This is because the small spatial scales responsible for turbulent dissipation also have a small time scale, much smaller than the buoyancy time scale of $1/N$. Beyond $x/D \approx 15$, buoyancy and transport dominate the $Fr = 1$ budget and balance one another.

Budget distributions are distinctive for all three simulated stratifications in the far wake as shown in Figure 7 (right column). The budget for the unstratified case remains similar to that of the intermediate wake where production is relatively small suggesting that the wake continues to behave as freely-decaying turbulence. In addition, advection is balanced by transport and dissipation. For $Fr = 3$, all terms are of the same order of magnitude. For both stratified cases, production has order of magnitude $O(10^{-5})$, two order of magnitude larger than in the unstratified case with $O(10^{-7})$. The dissipation takes similar values in the $Fr = 3$ and 1 wakes. At $Fr = 1$, buoyancy and transport remain dominant. This is contrary to the $t.k.e.$ budget for $Fr = 1$ at lower $Re = 3700$ presented in Pal et al. (2017) where the buoyancy term is balanced by the advection term in the far-wake.

Acknowledgments

REFERENCES

Balaras, Elias 2004 Modeling complex boundaries using an external force field on fixed cartesian grids in large-eddy simulations. *Comput. Fluids* **33**, 375–404.

Bonnier, M. & Eiff, O. 2002 Experimental investigation of the collapse of a turbulent wake in a stably stratified fluid. *Phys. Fluids* **14** (2), 791–801.

Brucker, K. A. & Sarkar, S. 2010 A comparative study of self-propelled and towed wakes in a stratified fluid. *J. Fluid Mech.* **652**, 373–404.

Chomaz, J. M., Bonneton, P. & Hopfinger, E. J. 1993 The structure of the near wake of a sphere moving horizontally in a stratified fluid. *J. Fluid Mech.* **254**, 1–21.

Chongsiripinyo, K, Pal, A & Sarkar, S 2017 On the vortex dynamics of flow past a sphere at Re= 3700 in a uniformly stratified fluid. *Physics of Fluids* **29** (2), 020704.

Constantinescu, G. & Squires, K. 2004 Numerical investigation of flow over a sphere in the subcritical and supercritical regimes. *Phys. Fluids* **16** (5), 1449–1466.

Diamessis, P. J., Spedding, G. R. & Domaradzki, J. A. 2011 Similarity scaling and vorticity structure in high Reynolds number stably stratified turbulent wakes. *J. Fluid Mech.* **671**, 52–95.

George, William K 1989 The self-preservation of turbulent flows and its relation to initial conditions and coherent structures. *Advances in turbulence* pp. 39–73.

Germano, M., Piomelli, U., Moin, P. & Cabot, W. H. 1991 A dynamic subgrid-scale eddy viscosity model. *Physics of Fluids A: Fluid Dynamics* **3** (7), 1760–1765.

Hunt, J.C.R, Wray, A.A. & Moin, P. 1988 Eddies, streams, and convergence zones in turbulent flows. *Tech. Rep.*. CTR.

Lilly, Douglas K 1992 A proposed modification of the germano subgrid-scale closure method. *Physics of Fluids A: Fluid Dynamics* **4** (3), 633–635.

Lin, J. T. & Pao, Y. H. 1979 Wakes in stratified fluids. *Ann. Rev. Fluid Mech.* **11**, 317–338.

Nedić, J., Vassilicos, J.C. & Ganapathisubramani, B. 2013 Axisymmetric turbulent wakes with new nonequilibrium similarity scalings. *Physical review letters* **111** (14), 144503.

Pal, A., Sarkar, S., Posa, A. & Balaras, E. 2016 Regeneration of turbulent fluctuations in low-Froude number flow over a sphere at Reynolds number of 3700. *J. Fluid Mech.* **804 R2**, 1–11.

Pal, A., Sarkar, S., Posa, A. & Balaras, E. 2017 DNS of stratified flow past a sphere at a subcritical Reynolds number of 3700 and moderate froude number (submitted). *J. Fluid Mech.* .

Rodríguez, I., Lehmkuhl, O., Borrell, R. & Oliva, A. 2013 Flow dynamics in the turbulent wake of a sphere at sub-critical reynolds numbers. *Computers & Fluids* **80**, 233–243.

Rossi, T. & Toivanen, J. 1999 A parallel fast direct solver for block tridiagonal systems with separable matrices of arbitrary dimension. *SIAM Journal on Scientific Computing* **20** (5), 1778–1793.

Spedding, G. R. 1997 The evolution of initially turbulent bluff-body wakes at high internal Froude number. *J. Fluid Mech.* **337**, 283–301.

Yang, J. & Balaras, E. 2006 An embedded-boundary formulation for large-eddy simulation of turbulent flows interacting with moving boundaries. *J. Comput. Phys.* **215**, 12–40.

Yun, G., Kim, D. & Choi, H. 2006 Vortical structures behind a sphere at subcritical Reynolds numbers. *Phys. Fluids* **18** (1), 5102.
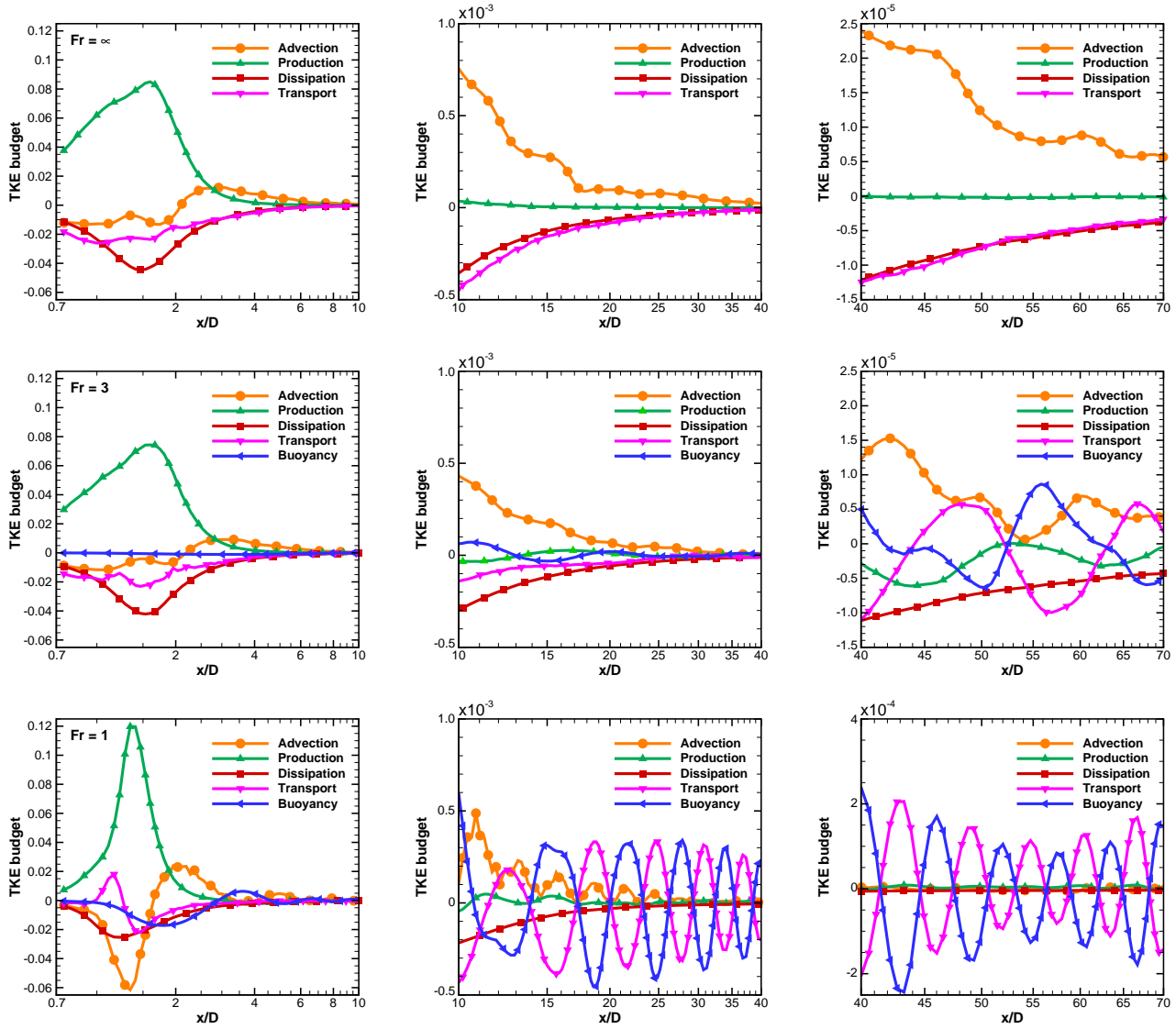
Figure 7. Terms in the *t.k.e.* budget for $Fr = \infty$ (top row), $Fr = 3$ (middle row), and $Fr = 1$ (bottom row) in the near-wake region $0.7 < x/D \leqslant 10$ (left column), the intermediate-wake region $10 < x/D \leqslant 40$ (middle column), and the far-wake region $40 < x/D \leqslant 70$ (right column).